

2 Electronic Structure of Correlated Materials: Slave-Boson Methods and Dynamical Mean-Field Theory

Gabriel Kotliar
Rutgers University
Piscataway, NJ, USA

Contents

1	First-principles approaches and model Hamiltonians	2
2	Slave-boson methods and emergence of local Fermi-liquids	6
3	DMFT for model Hamiltonians: Embedding and truncation	8
4	Correlations in the solid state, LDA, hybrids, LDA+DMFT	10
5	Electronic structure methods from a diagrammatic many-body perspective	13
6	Discretization of basis-sets and Coulomb integrals	15
7	Bridging between first-principles and model Hamiltonian approaches	18
8	Applications: Iron pnictides and Hund's metals	20
9	Applications: Actinides	23
10	Summary and outlook	24

1 First-principles approaches and model Hamiltonians

The standard model of solid state physics, described in solid state textbooks, has been extraordinarily successful in describing the properties of simple metals, semiconductors, and insulators. It is firmly grounded in the Landau Fermi Liquid Theory and perturbative expansions around the, by now standard, implementations of the density-functional theory (DFT), such as the Local-Density Approximation (LDA) or Generalized-Gradient Approximations (GGA) by means of the *GW* method.

Strongly correlated electron systems are materials that fall outside the standard model. They display remarkable phenomena ranging from high-temperature superconductivity in iron pnictides and copper-oxides, huge volume collapses in the $4f$ and $5f$ elemental series, to metal-to-insulator transitions in many transition-metal oxides such as V_2O_3 and VO_2 , to name a few.

From a theoretical perspective, these systems display remarkable emergent phenomena that cannot be accessed by perturbation theory starting from the band limit. Strong correlation phenomena require a different reference frame for their description and a methodology that is quite different from what is learned in traditional solid-state or many-body physics courses. Forty years ago, the theoretical toolbox to treat strong correlations was very limited. The focus was on variational wave functions of the type written by Gutzwiller [1] as used in the mixed-valence problem by Varma and Yaffet [2] and on the decoupling of equations of motion used by Hubbard [3]. Development of renormalization group methods for simple condensed matter physics problems was just beginning [4]. Methods for treating the unusual excitation spectra and the finite-temperature properties of strongly correlated materials were badly needed. At that time, we could not even contemplate a realistic treatment nor even a system-specific study of actual strongly correlated materials. The situation is completely different today, and the methods that brought about this change are the subject of these introductory notes, compiled by Wenhui Xu from lectures delivered by the author. They are intended as an orientation for beginning students in the field of electronic-structure calculations of strongly correlated materials. Their goal is to motivate students to enter the field by highlighting a couple of research achievements, rather than provide a complete overview with a complete list of references which can be found in the excellent collection of reviews in *Reviews of Modern Physics* [5–7]. The focus is on methods that target not only total energies, but finite-temperature properties and, most important, correlation functions.

Modern electronic-structure methods that treat correlated materials have developed into theoretical spectroscopies. This allows detailed comparison with experiments, which in turn catalyzes further theoretical progress. This iterative feedback loop is one of the characteristic strengths of condensed matter physics. Hence, some comparisons to experimental results are included in this lecture. While they convey some sense of collective achievement, they should also be a reminder that the theory of strongly correlated electron systems is still in its infancy. The goal is to highlight, in broad strokes, some advances that have taken place while indicating some problems that remain to be tackled to pave the way for a predictive theory of strongly correlated materials.

Historically, there have been two approaches to understanding and describing the physical properties of strongly correlated materials. First-principles (also called *ab-initio*) methods begin from the full Hamiltonian of electrons in the solid. This *theory of everything* is given by

$$H = \sum_i \frac{\nabla_i^2}{2m_e} + \sum_\alpha \frac{\nabla_\alpha^2}{2m_\alpha} - \sum_{\alpha,i} \frac{Z_\alpha e^2}{|\vec{R}_\alpha - \vec{R}_i|} + \frac{1}{2} \sum_{i \neq j} \frac{e^2}{|\vec{R}_i - \vec{R}_j|} + \frac{1}{2} \sum_{\alpha \neq \beta} \frac{Z_\alpha^2 e^2}{|\vec{R}_\alpha - \vec{R}_\beta|} + \text{relativistic effects.} \quad (1)$$

Here i and j are indices of electrons; α and β are indices of nuclei. Relativistic effects include spin-orbit coupling and are actually very important and give rise to qualitatively new physics in strongly correlated materials. One term, $\sum_i \frac{\vec{l}_i \cdot \vec{s}_i}{R_i^3}$, is essential to have non zero magnetocrystalline anisotropy, which selects the magnetization axis in crystals. We will not consider these terms in the lectures. We treat ions as very heavy objects (*adiabatic approximation*). In this limit $\sum_{\alpha,\beta} \frac{Z_\alpha Z_\beta e^2}{|\vec{R}_\alpha - \vec{R}_\beta|^2}$ becomes a number and $\sum_{\alpha,i} \frac{Z_\alpha e^2}{|\vec{R}_\alpha - \vec{R}_i|^2} \equiv \sum_i V_{\text{crystal}}(R_i)$ becomes an external potential for the electrons. Fluctuations around the equilibrium positions give rise to the lattice vibrations (phonons). Therefore, with these approximations Z_α and \vec{R}_α are the only input parameters, and approaches starting from Eq. (1) are referred to as first principles methods.

The standard model of solid state physics is grounded on two firm pillars. The first is the Fermi liquid theory, which justifies the use of free electrons as a reference system to describe the properties of an interacting Fermi system. In its renormalization group formulation [8], this can be understood by the statement that, in many instances, the interactions flow rapidly to zero as one approaches the Fermi surface. Then, below a certain scale, materials behave as non-interacting electrons, since the interactions have renormalized away. The only interactions that remain are Hartree-like terms that renormalize the responses to external fields (Landau Parameters). When this Fermi liquid scale is much larger than the temperatures of interest, the textbook picture of free fermions, in the presence of a periodic Bloch potential with renormalized parameters is thus justified.

The second pillar of the standard model enables the actual calculation of the quasiparticle dispersions and Fermi liquid parameters. It starts with the Kohn-Sham formulation [9] of density functional theory. It states the existence of a potential $V_{\text{KS}}(r)$, which is itself a functional of the density. One should write $V_{\text{KS}}(\vec{r})[\{\rho(\vec{r}')\}]$ to indicate this dependence, but we omit this in the following. The exact (but unknown) functional is such that the solution of the set of self-consistent equations,

$$[-\nabla^2 + V_{\text{KS}}(\vec{r})] \psi_{\vec{k}j}(\vec{r}) = \varepsilon_{\vec{k}j} \psi_{\vec{k}j}(\vec{r}). \quad (2)$$

$$\sum_{\vec{k}j} |\phi_{\vec{k}j}(\vec{r})|^2 f(\varepsilon_{\vec{k}j}) = \rho(\vec{r}) \quad (3)$$

reproduces the density of the solid. It is useful to divide the Kohn-Sham potential into several parts: $V_{\text{KS}} = V_{\text{Hartree}} + V_{\text{cryst}} + V_{xc}$, where one lumps into V_{xc} exchange and correlation effects beyond Hartree.

The eigenvalues $\varepsilon_{\vec{k}j}$ of the solution of the self-consistent set of Eq. (2) and (3) are not to be interpreted as excitation energies. The excitation spectra should be extracted from the poles of the one particle Green's function

$$G(\omega) = \frac{1}{[\omega + \nabla^2 + \mu - V_{\text{Hartree}} - V_{\text{cryst}}] - \Sigma(\omega)}. \quad (4)$$

Here μ is the chemical potential and we have singled out in Eq. (4) the Hartree potential expressed in terms of the exact density and the crystal potential, and lumped the rest of the effects of the correlation in the self-energy operator, which depends on frequency as well as on two space variables.

In a weakly correlated material, the one-particle excitation spectrum is perturbatively connected to the LDA Kohn-Sham spectrum, in the sense that the first-order correction in the screened Coulomb interactions for the self-energy Σ_{GW} (see the diagrams in figure 1) is such that $\Sigma = \Sigma_{GW} - V_{xc}$ is relatively small and able to bring the spectra sufficiently close to the experimental results. In fact, we can *define* weakly correlated materials as those solids for which the previous statement is true. Lowest order perturbation theory in the screened Coulomb interactions is called the *GW* method [10]. It has been very successful in predicting the trends of the gaps in semiconducting materials [11]

The *GW* method involves several steps, summarized in the diagrams shown in Fig. 1.

1. Computation of the polarization bubble

$$\Pi(t, t') = G_0(t, t') G_0(t', t). \quad (5)$$

2. Evaluation of the screened Coulomb potential W in random-phase approximation (RPA)

$$W^{-1} = v_{\text{Coul}}^{-1} - \Pi. \quad (6)$$

where v_{Coul} is the bare Coulomb potential.

3. Evaluation of the Σ_{GW} contribution to self-energy by lowest-order perturbation theory in W ; it is given in real space by (see Fig. 1)

$$\Sigma_{GW} = G_0 W. \quad (7)$$

4. From the self-energy one obtains the full Green's function using the Dyson equation where one removes the V_{xc} term from G_0 and adds the *GW* contribution to the self-energy to obtain an approximation to Eq. (4)

$$G^{-1} = G_0^{-1} - \Sigma. \quad (8)$$

We have not yet specified what one should take for G_0 in this algorithm. Various ideas have been discussed and implemented, leading to different variants of the *GW* method. In the ‘‘one-shot’’ *GW* method one uses the LDA Kohn-Sham Green's function

$$G_0(i\omega)^{-1} = i\omega + \mu + \nabla^2 - V_{\text{Hartree}} - V_{\text{cryst}} - V_{xc}^{\text{LDA}}. \quad (9)$$

and the self-energy is thus taken to be $\Sigma = \Sigma_{GW} - V_{xc}^{\text{LDA}}$.

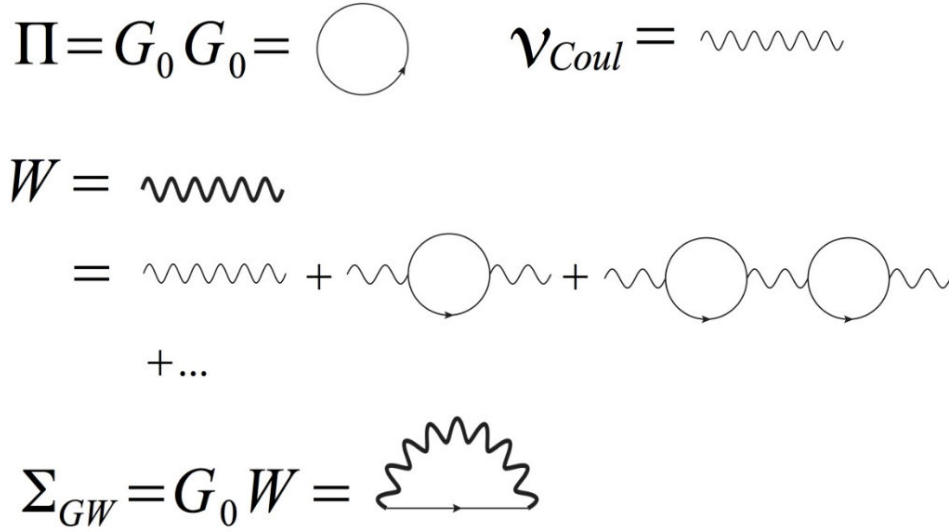


Fig. 1: Schematic diagrams for the GW method. Starting from some G_0 , a polarization bubble is constructed, which is used to screen the Coulomb interactions resulting in an interaction W . This W is then used to compute a self-energy Σ_{GW} using W and G_0 . To obtain the full Green's function G in Eq. (4), one goes from Σ_{GW} to Σ by subtracting the necessary single-particle potential and uses the Dyson equation $G^{-1} = G_0^{-1} - \Sigma$ as discussed in the text.

In the original self-consistent scheme proposed by Hedin [10] (the self-consistent GW) $G_0 = G$ is used and in this case $V_{xc} = 0$ is not needed and is not used in intermediate steps. There are numerous advantages, however, in using a non-interacting form for G_0 in the algorithm. In the quasi-particle self-consistent GW (QP-GW) [11] the “best” non-interacting Green's function is used for G_0 which uses an “exchange and correlation potential” V_{xc}^{QP-GW} chosen to reproduce the same quasiparticle spectra as the full GW greens function.

$$G_0(i\omega)^{-1} = i\omega + \mu + \nabla^2 - V_{\text{Hartree}} - V_{\text{cryst}} - V_{xc}^{QP-GW}. \quad (10)$$

The GW or RPA method captures an important physical effect. Electrons are charged objects that interact via the long range Coulomb interactions. Quasiparticles, on the other hand, are neutral. They are composed of electrons surrounded by screening charges, thus reducing the strength and the range of their interaction. For this reason, in many model Hamiltonians describing metals, only the short range repulsion is kept. To get a feeling for the screening effect, let's evaluate Eqs. (5) and (6) for an effective interaction W in the case that there is only one band of electrons with dispersion ε_k

$$\begin{aligned}
 \Pi(i\Omega = 0, \vec{q}) &= T \sum_{\omega} \sum_{\vec{k}} \frac{1}{i\omega - \varepsilon_{\vec{k}+\vec{q}}} \frac{1}{i\omega - \varepsilon_{\vec{k}}} = \sum_{\vec{k}} \frac{f(\varepsilon_{\vec{k}+\vec{q}}) - f(\varepsilon_{\vec{k}})}{\varepsilon_{\vec{k}+\vec{q}} - \varepsilon_{\vec{k}}} \\
 &\simeq - \sum_{\vec{k}} \left(\frac{\partial f(\varepsilon)}{\partial \varepsilon} \right)_{\varepsilon_{\vec{k}}} \simeq \sum_{\vec{k}} \delta(\varepsilon_{\vec{k}}) = \rho_{DOS}, \quad (11)
 \end{aligned}$$

where ρ_{DOS} is the density of states at the Fermi surface.

In momentum space, $v_{Coul}(\vec{q}) = 4\pi e^2/q^2$. Then

$$W(\vec{q}) = \frac{v_{Coul}(\vec{q})}{1 + v_{Coul}(\vec{q})\rho_{DOS}} \simeq \frac{1}{q^2 + 4\pi e^2\rho_{DOS}} \quad (12)$$

and its Fourier transform $W(\vec{r})$, which is now a function of one variable due to translation invariance, decays exponentially in space.

Model Hamiltonians are simplified Hamiltonians describing a reduced set of degrees of freedom, and involve a number of parameters. They are extremely useful for learning the qualitative physics exhibited by strongly correlated materials. Conceptually, we can obtain model Hamiltonians by selecting low-energy degrees of freedom (usually a few bands) and describing their interactions, which in metals at low energies are short-ranged due to the screening mechanism. The most famous example is the multi-orbital Hubbard model.

$$H = \sum_{i,j} c_{\alpha}^{\dagger}(i) t_{ij}^{\alpha\beta} c_{\beta}(j) + \sum_i U_{\alpha\beta\gamma\delta} c_{\alpha}^{\dagger}(i) c_{\beta}^{\dagger}(i) c_{\gamma}(i) c_{\delta}(i). \quad (13)$$

Even simplified model Hamiltonians have proved to be very difficult to solve exactly in the thermodynamical limit except for the cases of one dimension [12] and the limit of infinite dimensions [13], a limit where Dynamical Mean-Field Theory (DMFT) becomes exact.

Another celebrated model, the Anderson Impurity Model, was introduced by Anderson in the sixties to describe transition-metal impurities in metallic hosts [14]. It will play an important role in the DMFT analysis of the Hubbard model in Sec. 3.

2 Slave-boson methods and emergence of local Fermi-liquids

The spectra of strongly correlated electron materials are very far from those of free fermions. The one electron spectral function $A(\vec{k}, \omega)$ displays not only a dispersive quasiparticle peak but also other features commonly denoted as satellites. The collective excitation spectra, which appear in the spin and charge excitation spectra, do not resemble the particle-hole continuum of the free Fermi gas, with additional collective modes (zero sound, spin waves) produced by the residual interactions among them. Finally, the damping of the elementary excitations in many regimes does not resemble that of a Fermi liquid.

The key idea of the slave-boson method is to enlarge the Hilbert space so as to be able to more explicitly introduce operators that closely describe the physical excitations.

This is done by reformulation of the Hamiltonian in terms of additional slave variables, with additional Lagrange multipliers that impose constraints. We illustrate this idea with the multi-orbital Hubbard model following Refs. [15] and [16]. We first focus on one site and on the local interaction term

$$H_{loc} = \sum_{\alpha} \varepsilon_{\alpha}^0 \hat{n}_{\alpha} + \sum_{\alpha\beta} U_{\alpha\beta} \hat{n}_{\alpha} \hat{n}_{\beta} \quad (14)$$

acting on a Hilbert space

$$|n\rangle = \left(d_1^{\dagger}\right)^{n_1} \cdots \left(d_M^{\dagger}\right)^{n_M} |vac\rangle. \quad (15)$$

We notice that Eq. (14) is equivalent to another Hamiltonian which acts on a larger Hilbert space on which we will impose some constraints to retrieve the original problem

$$|\underline{n}\rangle \equiv \phi_n^\dagger |vac\rangle \otimes |n\rangle_f, \quad (16)$$

$$|n\rangle_f \equiv \left(f_1^\dagger\right)^{n_1} \cdots \left(f_M^\dagger\right)^{n_M} |vac\rangle. \quad (17)$$

The states in the original Hilbert space, denoted by a bar, are in one-to-one correspondence with the states of the enlarged Hilbert space once the constraints

$$\sum_n \phi_n^\dagger \phi_n = 1, \quad (18)$$

$$\sum_n n_\alpha \phi_n^\dagger \phi_n = f_\alpha^\dagger f_\alpha, \quad \forall \alpha \quad (19)$$

are imposed. In the enlarged Hilbert space, the physical electron is described by

$$\underline{d}_\alpha^\dagger = R_\alpha[\phi] f_\alpha^\dagger, \quad (20)$$

where

$$R_\alpha[\phi] = \sum_{nm} \langle n | f_\alpha^\dagger | m \rangle \left[\hat{\Delta}_\alpha \right]^{-1/2} \phi_n^\dagger \phi_m \left[1 - \hat{\Delta}_\alpha \right]^{-1/2} \quad (21)$$

with

$$\hat{\Delta}_\alpha[\phi] \equiv \sum_n n_\alpha \phi_n^\dagger \phi_n. \quad (22)$$

The kinetic energy is then

$$\underline{H} = \sum_{ij} R_\alpha[\phi] f_\alpha^\dagger(i) t_{ij}^{\alpha\beta} R_\beta[\phi] f_\beta(j). \quad (23)$$

while the local energy and interaction terms in the enlarged Hilbert space are reproduced by a quadratic Hamiltonian

$$H_{loc} = \sum_n \phi_n^\dagger \phi_n \varepsilon_n \quad (24)$$

where $\varepsilon_n = \sum_\alpha (n_\alpha + \sum_\beta U_{\alpha\beta} n_\alpha n_\beta)$.

The fact that the Hamiltonian is now quadratic in bosons and fermions suggests simple approximations for its treatment. The square root factors are largely arbitrary, in the sense that they only affect the degrees of freedom outside the physical Hilbert space, and they were chosen so as to give the same results as the Gutzwiller approximation and have a simple probabilistic interpretation.

The self-energy of the Green's function that results from the mean-field approximation (replacing ϕ 's and Lagrange multipliers λ by numbers) has the form

$$\Sigma_\alpha(\omega) = \Sigma_\alpha(0) + \omega \left(1 - \frac{1}{Z_\alpha} \right), \quad (25)$$

where

$$Z_\alpha = |R_\alpha|^2, \quad (26)$$

and

$$\Sigma_\alpha(0) = \lambda_\alpha / |r_\alpha|^2 - \varepsilon_\alpha^0. \quad (27)$$

Hence this theory describes the emergence of a local Fermi liquid. Non-local self-energies can be obtained with the significant extension introduced in Ref. [17].

This formulation explicitly exhibits the local collective modes (local charge, spin, and orbital fluctuations) in terms of the slave-boson operators. It has been extended [17–19] to make it manifestly rotationally invariant. For example, in the one-band Hubbard model in the simple slave-boson formulation, the state with one spin is described by the slave-boson ϕ_σ and transforms according to the fundamental representation of $SU(2)$. The spin fluctuations are naturally described by objects that transform according to the adjoint representation of $SU(2)$, which requires a matrix representation of the slave particles. Another advantage of the rotationally invariant formulation [17] is that it allows the treatment of realistic Hamiltonians including general multiplet interactions.

The physical electron operator is now represented in the enlarged Hilbert space by

$$\underline{d}_\alpha = \hat{R}_{\alpha\beta}[\phi] f_\beta. \quad (28)$$

At the mean-field level, \hat{R} has the interpretation of the quasiparticle residue, exhibiting the strong renormalizations induced by the electronic correlations. An important feature of the rotationally invariant formalism is that the basis that diagonalizes the quasiparticles represented by the operators f is not necessarily the same basis as that which would diagonalize the one electron density matrix expressed in terms of the operators d and d^\dagger . Strongly renormalized fermionic quasiparticles emerge in this treatment. This slave-boson formulation [15], reproduces at the saddle point level the results of the Gutzwiller approximation. Fluctuations around the saddle point generate the Hubbard bands in the one-particle spectra [20]. This method can be applied to the Anderson impurity model. When supplemented by the DMFT self-consistency condition, it gives the same results as its direct application to the lattice [21]. We envision many synergistic applications of the slave-boson technique and exact implementations of the DMFT, and we will return to this perspective at the end of Sec. 9.

3 DMFT for model Hamiltonians: Embedding and truncation

Dynamical mean field theory [22] is the natural extension of the Weiss mean-field theory of spin systems to treat quantum mechanical model Hamiltonians. It involves two steps. The first step focuses on a single lattice site and describes the rest of the sites by a medium with which an electron at this site hybridizes. This *truncation* to a single site problem is common to all mean-field theories. In the Weiss mean-field theory one selects a spin at a given site and replaces the rest of the lattice by an effective magnetic field or Weiss field. In the dynamical mean-field theory, the local Hamiltonian at a given site is kept, and the kinetic energy is replaced

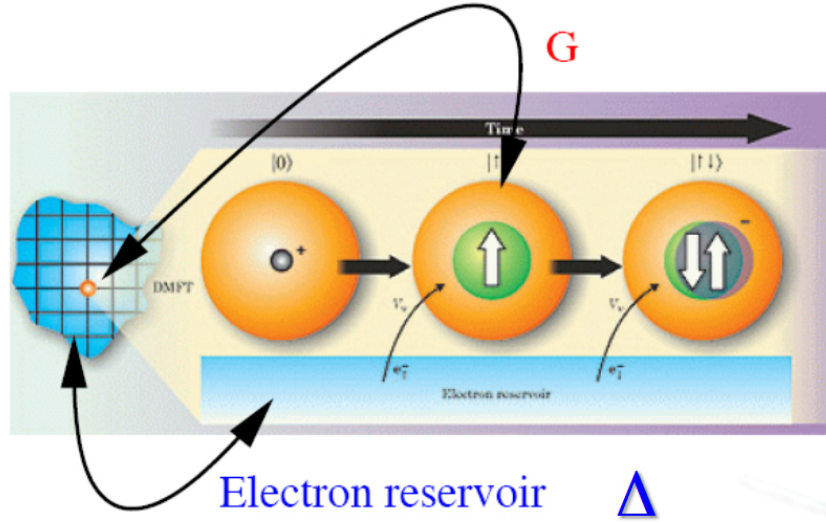


Fig. 2: Dynamical Mean-Field Theory (DMFT) maps (or truncates) a lattice model to a single site embedded in a medium (impurity model) with a hybridization strength that is determined self-consistently. Adapted from Ref. [23]

Weiss mean field theory	dynamical mean-field theory
Ising model → single spin in an effective Weiss field	Hubbard-type model → impurity in an effective bath
Weiss field: h_{eff}	effective bath: $\Delta(i\omega_n)$
local observable: $m = \langle s_i \rangle$	local observable: $G_{loc}(i\omega_n)$
self-consistent condition: $\tanh\left(\beta \sum_j J_{ij} s_j\right) = m$	self-consistent condition: $i\omega_n - E_{imp} - \Delta(i\omega_n) - \Sigma(i\omega_n) = \left[\sum_{\vec{k}} G_{\vec{k}}(i\omega_n)\right]^{-1}$

Table 1: Corresponding quantities in dynamical mean-field theory (right) and Weiss or static mean-field theory in statistical mechanics (left).

by a hybridization term with a bath of non-interacting electrons, which allows the atom at the selected site to change its configuration. This is depicted in Fig. 2.

The second step involves the reconstruction of lattice observables by *embedding* the local impurity self-energy into a correlation function of the lattice. $G_{latt}(\vec{k}, i\omega)^{-1} = i\omega + \mu - t_{\vec{k}} - \Sigma_{imp}(i\omega)$. Here $\Sigma_{imp}(i\omega)$ are viewed as functionals of the Weiss field. The requirement $\sum_{\vec{k}} G_{latt} = G_{loc}$ determines the Weiss field. Table 1 summarizes the analogies between Weiss mean-field theory and dynamical mean-field theory.

The DMFT mapping of a lattice model onto an impurity model gives a local picture of the solid in terms of an impurity model, which then can be used to generate lattice quantities, such as the Green's function of electrons and the magnetic susceptibility, by computing the corresponding irreducible quantities. This is illustrated in Fig. 3.

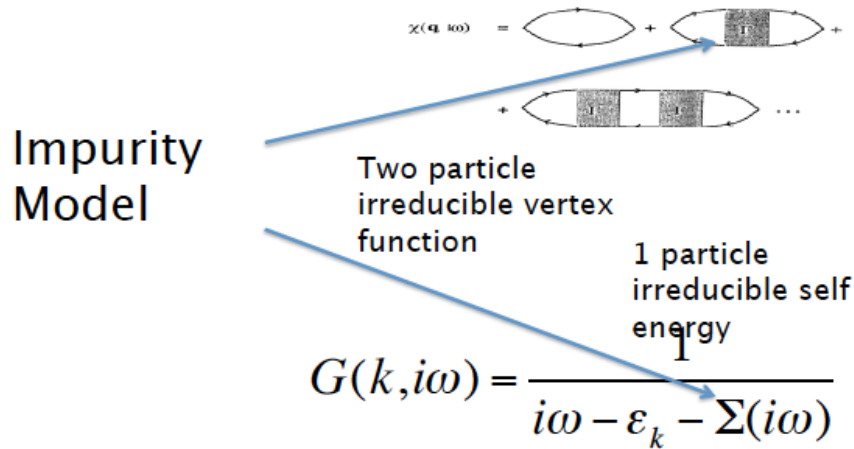
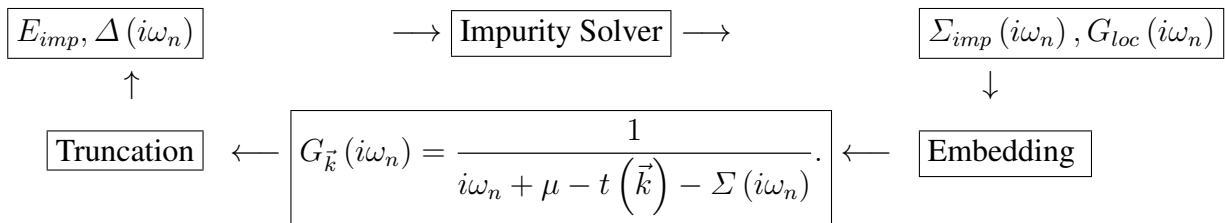


Fig. 3: The DMFT impurity model is used to generate irreducible quantities such as self-energies and two-particle vertices. These are then embedded in the lattice model to generate momentum dependent lattice quantities such as spectral functions or spin susceptibilities.

The self-consistent loop of DMFT is summarized in the following iterative cycle



The impurity model is the engine of a DMFT calculation. Multiple approaches have been used for its solution, and full reviews are needed to do this topic justice. Recent advances in the continuous-time quantum Monte Carlo method for impurity models [24] have provided numerically exact solutions at relatively low computational cost. Dynamical mean-field theory becomes exact in the limit of infinite dimensions that was introduced by Metzner and Vollhardt [13]. With suitable extensions, it plays an important role in realistically describing strongly correlated materials. This is the subject of the following sections.

4 Correlations in the solid state, LDA, hybrids, LDA+DMFT

In the context of the simple Hubbard model, a clear measure of the strength of the electronic correlations is the ratio U/t . But how do we quantify correlation-strength in an actual solid described by Eq. (1), which has no reference to a U or a t ?

To address this question we need to start from the exact one-particle Green's function in the solid that we introduced in Eq. (4) and focus on the self-energy Σ which should be viewed as an infinite-dimensional matrix in a specified basis set.

For a chemist, correlations mean large departures of Σ with respect to the Fock self-energy. Hence, a strongly correlated system is a system where $\Sigma - \Sigma_{Fock}$ is large. From this perspective,

even simple metals are strongly correlated since pure exchange is a poor approximation to the self-energy of even simple metals.

We adopt a different definition, the one used by physicists, and measure the strength of the correlation by the departure of the self-energy from the exchange-correlation potential of the LDA. A correlated material is one where

$$\Sigma(\omega) - V_{xc(LDA)} \quad (29)$$

is large in some *low* frequency range. Notice that at infinite frequencies Σ is given by just the Fock diagram and therefore at large frequencies the difference in Eq. (29) is large, but this usually occurs above the plasma frequency, a fairly large energy scale.

Sometimes the difference in Eq. (29) is local and restricted to a few orbitals, as will be explained in the following. In this case we can describe this difference using DMFT. This is the basis of the DFT+DMFT methodology, to be described below. Notice, however, that this methodology should be used as a description of the spectra below the plasma frequency.

Introducing a complete basis set of localized wavefunctions labeled by site and orbital index, we can expand the self-energy as

$$\Sigma(\vec{r}, \vec{r}', \omega) = \sum_{\alpha\vec{R}, \beta\vec{R}'} \chi_{\alpha\vec{R}}^*(\vec{r}) \Sigma(\omega)_{\alpha\vec{R}, \beta\vec{R}'} \chi_{\beta\vec{R}'}(\vec{r}'). \quad (30)$$

Eq. (30) allows us to introduce an approximate or simplified representation of the self-energy [25] involving a sum of a non-local but frequency independent term plus a frequency-dependent but local self-energy.

$$\Sigma(\vec{k}, \omega) \simeq \Sigma(\vec{k}) + \sum_{\vec{R}, \alpha\beta \in L} |\vec{R}\alpha\rangle \Sigma(\omega)_{loc, \vec{R}\vec{R}} \langle \vec{R}\beta|. \quad (31)$$

Notice that the notion of locality is defined with reference to a basis set of orbitals. The self-energy is approximately local when the on-site term $\vec{R} = \vec{R}'$ in Eq. (30) is much larger than the rest, and the ansatz is useful when the sum over orbitals in Eq. (31) runs over a small set L (much smaller than the size of the basis set), for example over a single shell of d - or f -orbitals. The validity of the local ansatz for graphs beyond the GW approximation was tested for transition metals in an LMTO basis set by N. Zein *et al.* [26].

For semiconductors, non-local (but frequency-independent) correlation effects are needed to increase the gap from its LDA value. This admixture of exchange can be done within the GW method or using hybrid density functionals. It reflects the importance of exchange beyond the LDA, which is due to the long-range but static part of the Coulomb interaction. It has recently been shown that this type of correlation effect is important in materials near a metal-to-insulator transition such as BaBiO_3 or HfClN [27]. In these systems, $\Sigma(\vec{k})$ is much more important than the frequency dependence in the self-energy.

Frequency dependence implies non-locality in time and is important in materials governed by Mott or Hund's physics. This physics tends to be local in space and can be captured by DMFT.

Static mean-field theories such as the LDA do not capture this non-locality in time, and therefore fail to describe Mott or Hund's phenomena.

In the quantum chemistry jargon the frequency-independent self-energy is ascribed to *dynamical* correlation effects, while the frequency-dependent self-energy is ascribed to *static* correlation effects. This difference in terminologies among two communities that are describing similar effects has been a continuous source of confusion. In real materials, both effects are present to some degree thus motivating physically the ansatz of Eq. (31). Some examples discussed recently are CeO₃ (using hybrid DFT+DMFT) in Ref. [28] and the iron pnictides and chalcogenides in Ref. [25].

This discussion motivates the DFT+DMFT method, which was introduced in Ref. [29] (see also Ref. [30]). DFT here stands for density-functional theory, and refers to the standard practical implementations of this theory, such as LDA or GGA, which are used with similar frequency. However DFT could be replaced by another static mean-field theory like hybrid DFT or QPGW. In the following we will use the terminology LDA+DMFT.

Starting from the model Hamiltonian point of view, one divides the orbitals into two sets, the first set containing the large majority of the electrons, which are properly described by the LDA Kohn-Sham matrix. The second set contains the more localized orbitals (*d*-electrons in transition metals and *f*-electrons in rare earths and actinides), which require the addition of DMFT corrections. A subtraction (called the double-counting correction) takes into account that the Hartree and exchange correlation has been included in that orbital twice since it was treated both in LDA and in DMFT. The early LDA+DMFT calculations proceeded in two steps (one-shot LDA+DMFT). First an LDA calculation was performed for a given material. Then a model Hamiltonian was constructed from the resulting Kohn-Sham matrix corrected by E_{DC} written in a localized basis set. The values of the Coulomb matrix for the correlated orbitals were estimated or used as fitting parameters. Finally DMFT calculations were performed to improve on the one-particle Green's function of the solid.

In reality, the charge is also corrected by the DMFT self-energy, which in turn changes the exchange and correlation potential away from its LDA value. Therefore charge self-consistent LDA+DMFT is needed.

For this purpose, it is useful to notice that the LDA+DMFT equations can be derived as stationary points of an LDA+DMFT functional, which can be viewed as a functional of the density and local Green's function of correlated orbitals. This is a spectral density-functional

$$\begin{aligned}
& \Gamma_{\text{DFT+DMFT}} \left[\rho(\vec{r}), G_{\alpha\beta, \vec{R}}, V_{KS}(\vec{r}), \Sigma_{\alpha\beta, \vec{R}} \right] \\
&= -\text{Tr} \ln \left[i\omega_n + \frac{\nabla^2}{2} - V_{KS} - \sum_{R, \alpha\beta \in L} \chi_{\alpha\vec{R}}^*(\vec{r}) \Sigma_{\alpha\beta\vec{R}}(i\omega) \chi_{\beta\vec{R}}(\vec{r}) \right] \\
&= \int V_{KS}(\vec{r}) \rho(\vec{r}) d^3r - \sum_n \text{Tr} [\Sigma(i\omega_n) G(i\omega_n)] + \int d^3r V_{\text{ext}}(\vec{r}) \rho(\vec{r}) d^3r \\
&= +\frac{1}{2} \int \frac{\rho(\vec{r}) \rho(\vec{r}')}{|\vec{r} - \vec{r}'|} d^3r d^3r' + E_{xc}^{\text{DFT}}[\rho] + \sum_{\vec{R}} \Phi \left[G_{\alpha\beta, \vec{R}}, U \right] - \Phi_{DC}. \quad (32)
\end{aligned}$$

Φ is the sum of two-particle irreducible diagrams written in terms of G and U . It was written down for the first time in Ref. [31] building on the earlier work of Chitra [32,33] and is essential for total energy calculations which require the implementation of charge self-consistency in the LDA+DMFT method. The first implementation of charge self-consistent LDA +DMFT was carried out in a full-potential LMTO basis set [31]. It was used to compute total energy and phonons of δ -plutonium.

The form of the LDA+DMFT functional makes it clear that the method is independent of the basis set used to implement the electronic structure calculation provided that the basis is complete enough. On the other hand, it is clearly dependent on the parameter U chosen, on the form of the double counting correction and the choice of the projector (i.e., the orbitals $\chi_\alpha(\vec{r})$ with $\alpha \in L$ that enter this definition). A projector of the form $P(r, r') = \sum_{\alpha\beta \in L} \chi_{\alpha\vec{R}}^*(\vec{r}) \chi_{\beta\vec{R}}(\vec{r}')$ was used to define a truncation from G to G_{loc} . The inverse of P is the embedding operator E defined by $P \cdot E = I_L$ where I_L is the identity operator in the correlated subspace. If one restricts $E \cdot P$ to the space L , one also obtains the identity operator in that space. E is used to define an embedding of the self-energy $\Sigma(r, r') = E^{\alpha,\beta}(r, r') \Sigma_{\alpha,\beta}^{loc}$.

However, more general projectors can be considered as long as causality of the DMFT equations is satisfied. Ideas for choosing an optimal projector for LDA+DMFT based on orbitals were presented in Ref. [34]. Choosing suitable projectors (and correspondingly a suitable value of the U matrix and a proper double counting correction) is crucial for the accuracy of an LDA+DMFT calculation as demonstrated recently in the context of the hydrogen molecule [35].

5 Electronic structure methods from a diagrammatic many-body perspective

The formulation of LDA+DMFT presented in the previous section is rooted in the model Hamiltonian approach, which contains parameters such as the screened Coulomb interaction matrix or hopping matrix elements. These elements are absent in the starting point of the first principles approaches Eq. (1). We now describe a route proposed by Chitra [32,33] to embed DMFT into a many-body approach of electronic structure within a purely diagrammatic approach formulated in the continuum.

The starting point once again is the theory of everything:

$$S = \int dx \psi^\dagger(x) [\partial_\tau - \nabla^2 + V_{\text{ext}}(x)] + \frac{1}{2} \int dx dx' \psi^\dagger(x) \psi^\dagger(x') v_{\text{Coul}}(x-x') \psi(x) \psi(x'), \quad (33)$$

which can be rewritten exactly in terms of a Hubbard-Stratonovich field $\phi(x)$ that represents the electric field present in the solid,

$$S = \int dx \psi^\dagger(x) [\partial_\tau - \nabla^2 + V_{\text{ext}}(x)] + \frac{1}{2} \int dx dx' \phi(x) v_{\text{Coul}}^{-1}(x-x') \phi(x') + \int dx i\phi(x) \psi^\dagger(x) \psi(x). \quad (34)$$

$$\Phi_{GW}(G, W) = \begin{array}{c} \text{---} G(\mathbf{r}\mathbf{r}') \\ \circlearrowleft \\ \vdots V_C \\ \circlearrowright \end{array} + \begin{array}{c} \text{---} G(\mathbf{r}\mathbf{r}') \\ \text{---} W(\mathbf{r}\mathbf{r}') \\ \text{---} G(\mathbf{r}\mathbf{r}') \end{array}$$

Fig. 4: Lowest order graphs in the Φ -functional of Eq. (37). They give rise to the fully self-consistent GW approximation.

From this action, one can compute the Green's function

$$G(x, x') = -\langle \psi(x) \psi^\dagger(x') \rangle \quad (35)$$

and

$$W(x, x') = \langle \phi(x) \phi(x') \rangle - \langle \phi(x) \rangle \langle \phi(x') \rangle, \quad (36)$$

which are the same symbols as used in the GW method [10].

The free energy of the solid can be written as an exact functional of $G(x, x')$ and $W(x, x')$ by means of a Legendre transformation and results in

$$\begin{aligned} \Gamma[G, W, \Sigma, \Pi] = & -\text{Tr} \ln [G_0^{-1} - \Sigma] - \text{Tr} [\Sigma G] + \frac{1}{2} \text{Tr} \ln [v_{\text{Coul}}^{-1} \Pi] \\ & - \frac{1}{2} \text{Tr} [\Pi W] + E_{\text{Hartree}} + \Phi[G, W]. \end{aligned} \quad (37)$$

This reformulation is exact but not practical unless some approximations are made on the functional Φ , defined as sum of all two-particle irreducible diagrams. The lowest order graphs of this functional are shown in Fig. 4, which reproduce the self-consistent GW approximation.

If one selects a projector, which allows us to define a local Green's function, it was suggested in Refs. [32, 33, 36] that one can perform a local approximation and keep only the local higher order graphs in selected orbitals $\Phi[G, W] \simeq \Phi_{\text{EDMFT}}[G_{\text{loc}}, W_{\text{loc}}, G_{\text{nonlocal}} = 0, W_{\text{nonlocal}} = 0] + \Phi_{GW} - \Phi_{GW}[G_{\text{loc}}, W_{\text{loc}}, G_{\text{nonlocal}} = 0, W_{\text{nonlocal}} = 0]$. Since the lowest graph is contained in the GW approximation, one should start from the second order graph and higher order.

These ideas were formulated and fully implemented in the context of a simple extended Hubbard model by Ping Sun and the author [37, 38]. An open problem in this area, explored in Ref. [38], is the level of self-consistency that should be imposed. As discussed in Sec. 1, this important issue is already present in the implementation of the GW method, and the work of Ref. [38] should be revisited using the lessons from the QPGW method [25].

The functional Φ can be viewed as the functional of an impurity model which contains a frequency-dependent interaction U , obeying the self-consistency condition

$$U^{-1} = W_{\text{loc}}^{-1} + \Pi_{\text{loc}}. \quad (38)$$

One can understand the successes of LDA+DMFT from the GW+EDMFT perspective. Consider a system such as cerium, containing light *spd*-electrons and heavier, more correlated, *f*-electrons. We know that for very extended systems, the *GW* quasiparticle band structure is a good approximation to the LDA band structure. Therefore the self-energy of a diagrammatic treatment of the light electrons can be approximated by the exchange-correlation potential of the LDA (or by other improved static approximations if more admixture of exchange is needed). Diagrams of all orders, but in a local approximation, are used for the *f*-electrons. In the full many-body treatment, Σ_{ff} is computed using skeleton graphs with G_{loc} and W_{loc} . To reach the LDA+DMFT equations, one envisions that, at low energies, the effects of the frequency dependent interaction $U(\omega)$ can be taken into account by a static U , which should be close to (but slightly larger than) $U(\omega = 0)$. The *f*-*f*-block of the Green's function now approaches $\Sigma_{ff} - E_{\text{DC}}$.

We reach the LDA+DMFT equations, with some additional understanding on the origin of the approximations used to derive them from the EDMFT+GW approximation as summarized schematically in

$$\Sigma_{GW+DMFT}(\vec{k}, \omega) \longrightarrow \begin{pmatrix} 0 & 0 \\ 0 & \Sigma_{ff} - E_{\text{DC}} \end{pmatrix} + \begin{pmatrix} V_{xc}[\vec{k}]_{spd,spd} & V_{xc}[\vec{k}]_{spd,f} \\ V_{xc}[\vec{k}]_{f,spd} & V_{xc}[\vec{k}]_{f,f} \end{pmatrix}. \quad (39)$$

Realistic implementations of combinations of *GW* and DMFT have not yet reached the maturity of LDA+DMFT implementations and are a subject of current research.

6 Discretization of basis-sets and Coulomb integrals

There are now a large number of implementations of LDA+DMFT in various electronic structure codes in progress and this is an active area of research. In this section we provide some background elementary material, to give the student a feeling for the various parameters that enter in these modern LDA+DMFT calculations. This involves one-electron ideas such as muffin-tin radii and augmentation spheres as well as atomic physics concepts such as Slater integrals. The applications described in Sec. 8 and Sec. 9 were carried out using the LDA+DMFT implementation of K. Haule described in Ref. [39]. Early studies mentioned in section Sec. 9 used the LMTO basis set and the implementation described in Ref. [31].

Eq. (2) is a partial differential equation. To solve it on a computer, a discretization is needed to reduce it to a finite matrix diagonalization problem. More generally, the Kohn-Sham matrix is infinitely dimensional and model Hamiltonians require some reduction to finite dimensional matrices to be used in conjunction with DMFT. This is generally done by introducing a basis set χ_i ,

$$\psi = \sum_i c_i \chi_i. \quad (40)$$

The Schrödinger equation becomes

$$\langle \chi_j | H | \chi_i \rangle = \sum_i c_i \langle \chi_j | H | \chi_i \rangle = \varepsilon \sum_i \langle \chi_j | \chi_i \rangle. \quad (41)$$

That is,

$$\sum_i h_{ji} c_i = \varepsilon \sum_i O_{ji} c_i. \quad (42)$$

$$\begin{cases} h_{ji} = \langle \chi_j | H | \chi_i \rangle = \langle \chi_j | -\nabla^2 + v_{\text{KS}}(\vec{r}) | \chi_i \rangle. \\ O_{ji} = \langle \chi_j | \chi_i \rangle \text{ (overlap matrix)} \end{cases} \quad (43)$$

The linear augmented plane wave (LAPW) [40, 41] method divides the space into two categories, the interstitial region (I) and the muffin-tin region (MT). The LAPW basis set is defined by

$$\chi_{\vec{k}, \vec{G}}(\vec{r}) = \begin{cases} e^{i(\vec{k} + \vec{G}) \cdot \vec{r}}, & \text{for } \vec{r} \in I; \\ \sum_{lm} a_{lm}(\vec{k}) \phi_{lm} + b_{lm}(\vec{k}) \dot{\phi}_{lm}, & \text{for } \vec{r} \in MT \end{cases} \quad (44)$$

In the interstitial region, plane waves constitute a natural basis. In the muffin-tin sphere, the basis set contains linear combinations of atomic-like wavefunctions $\phi_{lm}(\vec{r}, E_\nu)$ and their derivatives, $\dot{\phi}_{lm}(\vec{r}, E_\nu)$, with respect to the energy parameter E_ν , which is called the linearization energy. The key idea is to allow enough variational freedom to reproduce the exact solution of the one-particle Schrödinger equation in the sphere [40]. The basis functions are

$$\phi_{lm}(\vec{r}, \varepsilon) = \phi_{lm}(\vec{r}, E_\nu) + (\varepsilon - E_\nu) \dot{\phi}_{lm}(\vec{r}, E_\nu), \quad (45)$$

where the atomic-like wavefunctions satisfy

$$[-\nabla^2 + V_{av}(\vec{r})] \phi_{lm}(\vec{r}, E_\nu) = E_\nu \phi_{lm}(\vec{r}, E_\nu) \quad (46)$$

and their derivatives with respect to E_ν satisfy

$$[-\nabla^2 + V_{av}(\vec{r})] \dot{\phi}_{lm} = \phi_{lm}. \quad (47)$$

Besides the one-particle Hamiltonian, one also needs to discretize the Coulomb interaction part of the Hamiltonian. We explain how this is done in the context of a single atom. In a model Hamiltonian language, the two most important terms are the Hubbard U , which suppresses charge fluctuations, and the Hund's rule coupling J , which promotes locally large values of spin

$$H_{\text{int}} \sim U \hat{N}^2 + J \hat{S}^2. \quad (48)$$

To see the origin of these terms we start from the atomic Hamiltonian with the Coulomb interaction written in second quantized form

$$\frac{1}{2} \int d^3r d^3r' \psi_\sigma^\dagger(\vec{r}) \psi_{\sigma'}^\dagger(\vec{r}') \frac{1}{|\vec{r} - \vec{r}'|} \psi_{\sigma'}(\vec{r}') \psi_\sigma(\vec{r}) = \frac{1}{2} \sum_{\alpha\beta\gamma\delta} c_{\alpha\sigma}^\dagger c_{\beta\sigma'}^\dagger \langle \alpha\beta | V | \gamma\delta \rangle c_{\delta\sigma'} c_{\gamma\sigma} \quad (49)$$

with

$$\langle \alpha\beta | V | \gamma\delta \rangle = \int d^3r_1 d^3r_2 \phi_\alpha^*(\vec{r}_1) \phi_\beta^*(\vec{r}_2) \frac{1}{|\vec{r}_1 - \vec{r}_2|} \phi_\delta(\vec{r}_2) \phi_\gamma(\vec{r}_1). \quad (50)$$

Using $\phi_{lm}(r, \vartheta, \varphi) = R_l(r) Y_{lm}(\vartheta, \varphi)$ and

$$\frac{1}{|\vec{r} - \vec{r}'|} = 4\pi \sum_{k=0}^{\infty} \frac{r_{<}^k}{r_{>}^{k+1}} \frac{1}{2k+1} \sum_{q=-k}^k Y_{kq}(\hat{r}) Y_{kq}^*(\hat{r}'), \quad (51)$$

we restrict ourselves to the d -shell ($l = 2$) as an example. The interaction has the form we encountered previously in the context of the multi-band Hubbard model, Eq. (13)

$$\sum_{m_1 m_2 m_3 m_4} \sum_{\sigma \sigma'} U_{m_1 m_2 m_3 m_4} c_{m_1 \sigma}^\dagger c_{m_2 \sigma'}^\dagger c_{m_3 \sigma'} c_{m_4 \sigma}, \quad (52)$$

Here U is a four-index tensor. In the atom, its form is strongly constrained by symmetries and is parametrized in terms of a few parameters (Slater integrals) F^k .

$$\begin{aligned} U_{m_1 m_2 m_3 m_4} &= \sum_k \frac{4\pi}{2k+1} \sum_{q=-k}^k \int d^3 r_1 \phi_{2m_1}^*(\vec{r}_1) \phi_{2m_4}(\vec{r}_1) Y_{kq}^*(\vartheta_1, \varphi_1) \\ &\quad \times \int d^3 r_2 \phi_{2m_2}^*(\vec{r}_2) \phi_{2m_3}(\vec{r}_2) Y_{kq}(\vartheta_2, \varphi_2) \times \frac{r_{<}^k}{r_{>}^{k+1}} \\ &= \sum_k F^k \sum_{q=-k}^k \langle Y_{2m_1} | Y_{kq}^* | Y_{2m_4} \rangle \langle Y_{2m_2} | Y_{kq} | Y_{2m_3} \rangle, \end{aligned} \quad (53)$$

and

$$F^k = \frac{4\pi}{2k+1} \int r_1^2 dr_1 \int r_2^2 dr_2 \frac{r_{<}^k}{r_{>}^{k+1}} R_{l=2}^2(r_1) R_{l=2}^2(r_2). \quad (54)$$

When $k = 0$ and hence $q = 0$, $\langle Y_{2m_1} | Y_{00}^* | Y_{2m_4} \rangle \propto \delta_{m_1 m_4}$ and $\langle Y_{2m_2} | Y_{00}^* | Y_{2m_3} \rangle \propto \delta_{m_2 m_3}$. The $k = 0$ contribution in the Coulomb interaction is

$$H_{Coul}^{k=0} \simeq F^0 \sum_{m, m'} \sum_{\sigma, \sigma'} (c_{m\sigma}^\dagger c_{m\sigma}) (c_{m'\sigma'}^\dagger c_{m'\sigma'}). \quad (55)$$

Thus, F^0 defines the Hubbard U in the atom. It involves the *direct* Coulomb integral U_{nmnmn} .

We now turn to the exchange Coulomb integral

$$U_{nmnmn} = \int d^3 r_1 d^3 r_2 \phi_m^*(\vec{r}_1) \phi_n(\vec{r}_1) \frac{1}{|\vec{r}_1 - \vec{r}_2|} \phi_n^*(\vec{r}_2) \phi_m(\vec{r}_2). \quad (56)$$

and its average $J = \frac{1}{2l+1} \sum_{m < n} U_{nmnmn}$. To understand its physical meaning consider the case that the full interaction is replaced by its more symmetric (averaged) form $U_{m_1 m_2 m_3 m_4} = J \delta_{m_1, m_3} \delta_{m_2, m_4} + \frac{J}{2} \delta_{m_1, m_4} \delta_{m_2, m_3}$. Then it is easy to evaluate the form of the interaction Hamiltonian using the Fierz identity $\sum_a \sigma^a_{\alpha\beta} \sigma^a_{\gamma\delta} + \delta_{\alpha\beta} \delta_{\gamma\delta} = 2\delta_{\alpha\delta} \delta_{\beta\gamma}$ to obtain

$$H \sim -2JS^2 \quad (57)$$

with $S^a = \frac{1}{2} \sum_{m, \alpha\beta} c_{m\alpha}^\dagger \sigma^a_{\alpha\beta} c_{m\beta}$. Notice the sign in Eq. (57), which gives rise to the famous Hund's rule: to minimize the energy one has to maximize the spin. The Hund's J for d -electrons can be expressed in terms of the Slater integrals [42] by

$$J = \frac{1}{14} (F^2 + F^4), \quad (58)$$

A second parameter in addition to J is needed to parametrize the Slater integrals

$$C = \frac{1}{14} \left(\frac{9}{7} F^2 - \frac{5}{7} F^4 \right) \quad (59)$$

When $C = 0$, additional symmetries are present in the spectra [43]. Sometimes F^2 and F^4 are viewed as parametrized by the Hund's coupling, as $F^2 \simeq \frac{14}{1.6} J$ and $F^4 \simeq \frac{0.6}{1.6} J$. This relation between F^2 and F^4 is exact only for the hydrogen atom. Note that in the case of instantaneous interactions, the terms of odd l , (F^1, F^3, \dots) are absent due to parity symmetry. Finally we give the expression for the atomic energy averaged over all the configurations for d -electrons

$$U_{av} = F^0 - \frac{2}{63} (F^2 + F^4). \quad (60)$$

The Hund's interaction is very important in determining the physical properties of many solids and we will return to this point in Sec. 8.

7 Bridging between first-principles and model Hamiltonian approaches

The ideas that we have pursued in this lecture are rooted in the philosophy of the Anderson model [14]. Many-body correlations are applied to a small subset of orbitals and are kept relatively local in space. The rationale, is that the large majority of electronic states can be treated accurately by some static mean-field plus low-order perturbative corrections, while a summation to all orders is only needed for a small subset of orbitals. This should be contrasted with other methods, such as GW or variational Monte Carlo where all electrons are treated at the same level of approximation. The advantage of LDA+DMFT-like approaches is that they focus the available computational power on the orbitals or sectors that need it the most. The disadvantage is that, like all methods rooted in model Hamiltonians, there is some arbitrariness that has to be resolved, for example in the determination of the form of the projector and the value of the concomitant interaction. The derivation of model Hamiltonians and their parameters can be carried out along two different lines.

The first is a Wilsonian approach, where high-energy degrees of freedom are eliminated. It involves the following schematic steps which results in a model Hamiltonian with well defined parameters:

1. start with the theory of everything in the path integral formulation
2. in metallic systems, screen the long range part of the Coulomb interaction
3. eliminate (integrate-out, approximately) degrees of freedom which are not of interest and therefore outside the scope of the model

A different philosophy for deriving parameters of low-energy Hamiltonian involves matching observables:

1. choose an approximate method
2. apply the method to the first-principle theory and the model
3. match enough quantities to determine (or over-determine) a few physical observables

An good example of this approach is the constrained RPA [44] proposed by Aryasetiawan and developed with his collaborators [45].

The model Hamiltonian will only keep bands within a low energy window near the Fermi surface as degrees of freedom of interest. The observables to be matched are the screened Coulomb interaction among the electrons W . The screened Coulomb potential in first-principle theory is given by

$$W = \frac{v_{\text{Coul}}}{1 + v_{\text{Coul}}\Pi} = \frac{v_{\text{Coul}}}{1 + v_{\text{Coul}}(\Pi_{\text{model}} + \Pi_{\text{rest}})}. \quad (61)$$

Π_{model} is the polarization of the low-energy bands. Π_{rest} is the polarization due to excitations between low- and high-energy bands and within the high-energy bands. The screened Coulomb potential in the model is

$$W_{\text{model}} = \frac{U}{1 + U\Pi_{\text{model}}}. \quad (62)$$

U is the “bare” interaction in the model Hamiltonian. The matching between the low energy theory and the full theory is

$$W = W_{\text{model}}, \quad (63)$$

which results in

$$\frac{U}{1 + U\Pi_{\text{model}}} = \frac{v_{\text{Coul}}}{1 + v_{\text{Coul}}(\Pi_{\text{model}} + \Pi_{\text{rest}})}, \quad (64)$$

leading to

$$U = \frac{v_{\text{Coul}}}{1 + v_{\text{Coul}}\Pi_{\text{rest}}}. \quad (65)$$

This is constrained RPA [44]. In general, $U(\omega; \vec{r}, \vec{r}')$ is a function of ω , \vec{r} , and \vec{r}' . Hence this method delivers both local and non-local frequency dependent interactions. Evaluating the results at zero frequency and projecting U on the relevant orbitals gives rise to the parameters of the model Hamiltonian.

A variant of this approach, a constrained local GW , was proposed in Ref. [46]. Here the observable to be matched is the local W , defined by projecting W onto local orbitals using the same projector to be used in DFT+DMFT. The matching equations are

$$W_{\text{loc}} = (W_{\text{model}})_{\text{loc}}, \quad (66)$$

$$\Pi_{\text{loc}} = (\Pi_{\text{model}})_{\text{loc}}, \quad (67)$$

which result in a different definition of the frequency dependent U in a solid

$$W_{\text{loc}}^{-1} = U^{-1} - \Pi_{\text{loc}} \quad (68)$$

The constrained RPA method, as GW , depends significantly on the level of self-consistency (one-shot, full self-consistency, or QPGW). It was observed in Ref. [46] that the one-shot approximation used in all earlier studies considerably underestimates the values of U that should

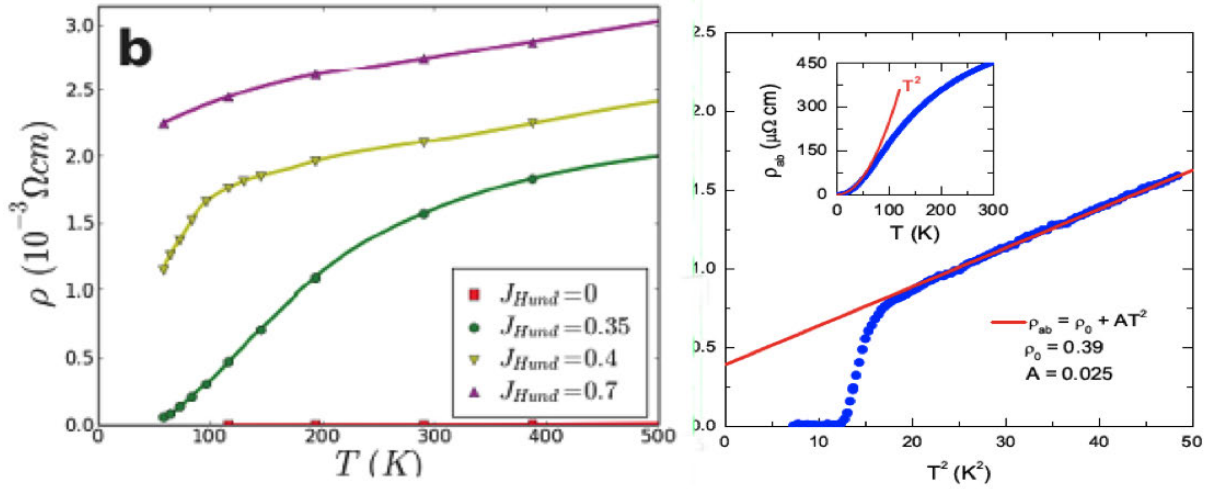


Fig. 5: (Left Panel) Resistivities as a function of Hund's rule coupling J , Ref. [50]. Notice the extreme sensitivity to J . The effects of U on the correlation strength are small even for values of U comparable to the bandwidth. The correlations are induced very rapidly by the Hund's J , and a coherence-incoherence crossover as a function of temperature was predicted. (Right Panel) Recent observation of this behavior in ultra-pure KFe_2As_2 [51].

be used together with a localized projector. On the other hand, the fully self-consistent GW which was implemented for solids in Ref. [47] gives instead fairly reasonable U values and total energies, while being less accurate than the QPGW and the one-shot GW for electronic spectra. Further investigations of this point in other materials are needed. Furthermore, the determination of the parameters and the type of projectors to be used in LDA+DMFT-like implementations remains a fundamental challenge in condensed matter physics.

8 Applications: Iron pnictides and Hund's metals

The field of correlated-electron materials continues to periodically produce surprising discoveries. The latest in the series is the high-temperature superconductivity in materials containing iron pnictide layers [48]. This recent development provided a unique opportunity to confront electronic structure methods with rapidly developing experiments and assess the predictive power of current methodologies and implementations. We use this as a first example in these lectures.

Shortly after the experimental discovery of the iron pnictides, it was determined that the electron-phonon coupling was not responsible for their superconductivity and correlations in the form of a mass enhancement (m^*/m between 3 and 5) were predicted [49]. Even more surprising was the *origin* of the mass enhancement which was elucidated in Ref. [50]. The left panel of Fig. 5 shows the crossover from coherence (Fermi-liquid behavior) at low temperatures to incoherence (bad-metal behavior) at high temperatures predicted in Ref. [49]. The right panel of Fig. 5 describes the evolution of the resistivity as a function of J , for a reasonably large value of the Hubbard U ($U=5$, comparable to the bandwidth). For small J , the system behaves as a weakly interacting material, with very low resistivity and negligible mass enhancement [49]. The rea-

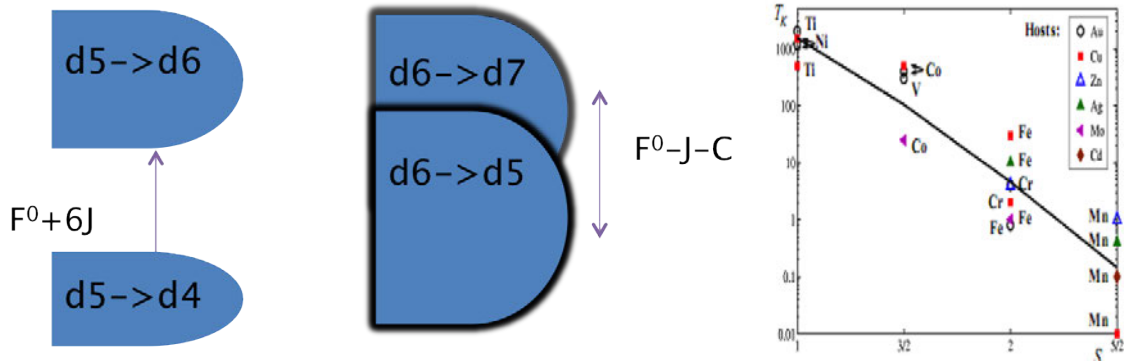


Fig. 6: J promotes metallicity in a d^6 configuration (middle) and insulating behavior in a d^5 configuration. The figure on the right shows the experimental dependence of the Kondo temperature on the d -valence [53]. It falls exponentially as the half filled shell (Mn) is approached.

son for this behavior is the very small value of the crystal-field splittings in the pnictides (of the order of ten meV as opposed to the value characteristic of oxides which is of the order of eV). The orbital degeneracy is then very large, with considerable room to move within the d -shell, rendering Mott blocking ineffective. In different words, the critical U for the Mott transition scales with N [52], ($U_{c2} \sim N^2$ and $U_{c1} \sim N$) and enormous values of U would be needed to induce Mott localization in this system.

The iron pnictide materials were therefore not just new high-temperature superconductors arising from a magnetic element. They were a new class of strongly correlated materials, where the correlations derive not from the blocking effect of the Mott Hubbard U , but from the effects of the Hund's rule coupling J . The theory of Hund's metals is not fully developed yet. Some basic understanding can be traced to the early work of van der Marel and Sawatzky [42], who observed that while in a half filled configuration such as Mn d^5 , Hund's rule J enhances the Mott Hubbard gap, in a d^6 configuration the Hund's rule J reduces the gap between the Hubbard bands, thus promoting metallicity, as shown in Fig. 6. Hundness is also clearly seen in the valence histogram, describing pictorially the diagonal elements of the local many body density matrix. Physically, it represents the fraction of the time that the shell spends in each different atomic eigenstate. It is shown in the right panel of Fig. 9 for BaFe_2As_2 . The material is clearly metallic with a very large number of configurations and several valences participating in the histogram. The Hund's J weights heavily the maximal spin states within each valence.

The Hund's coupling also has a dramatic impact at low energies. This has been known from the studies of magnetic impurities in transition-metals which were discussed intensively in the 1960s [54]. The Kondo temperature of transition metals decreases dramatically as it approaches the half-filled shell as shown in the right panel of Fig. 6. This can be understood as a result of the blocking of the orbitals which reduces the Kondo interaction to a diagonal form. The Kondo scale is exponential in the Kondo coupling. In a $SU(2N)$ -symmetric situation, containing only the interaction U , the Kondo scales as $\exp(-1/J\rho N)$ where N is the orbital degeneracy. Introduction of Hund's coupling removes the degeneracy from $SU(N)$ to $SU(2)$, and renormalizes the Kondo-coupling from J to J/N , resulting in a Kondo scale $\exp(-N/J\rho)$. These con-

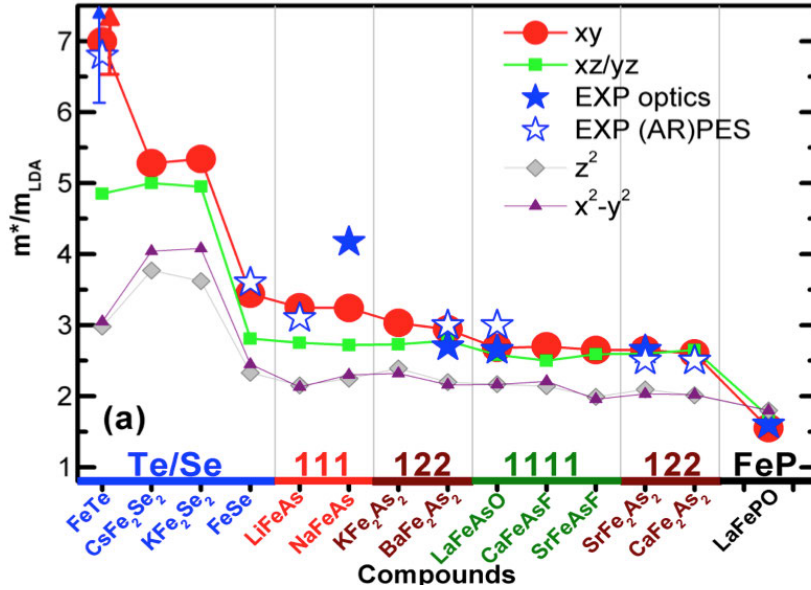


Fig. 7: Effective masses across the families of iron pnictides. All calculations were performed with fixed F^0 , F^2 , F^4 , and double-counting correction parameters. The variations in correlation strength agree reasonably well with experiment and can be traced to the position of the pnictogen height.

siderations are suitable for understanding the half-filled situation [55]. A full weak-coupling renormalization group treatment of the impurity model underlying the Hund's metal was only given very recently [56].

The question of whether the iron pnictides should be thought of as weakly correlated itinerant magnets, doped Mott insulators, or Hund's metals continues to be actively debated in the community. An important question is what controls the strength of the correlations within LDA+DMFT. At this point, technical advances in implementation finally enable the calculation of physical properties for whole families of compounds as illustrated in Fig. 7 from Ref. [57].

A big advantage of this type of calculation is that while absolute values of physical quantities are very sensitive to the strength of the Hund's coupling, this quantity is not expected to vary much from material to material and can be kept fixed as the chemical trends across similar materials are examined. This type of calculation clarified early confusion which classified some iron pnictides such as the 1111 system as weakly correlated, while placing others such as the 122 system in the strong correlation regime as a result of variations in the atomic parameters and double-counting corrections. This unified picture of the iron pnictide families was also confirmed by subsequent experimental optical studies.

The other factor that controls the strength of the interaction in the iron pnictides is the variation of the pnictide valence, with the correlation strength being an increasing function of decreasing valence. Arguments in favor of this point of view, in a very itinerant picture of Hund's metals, was advanced in Refs. [56] and [58].

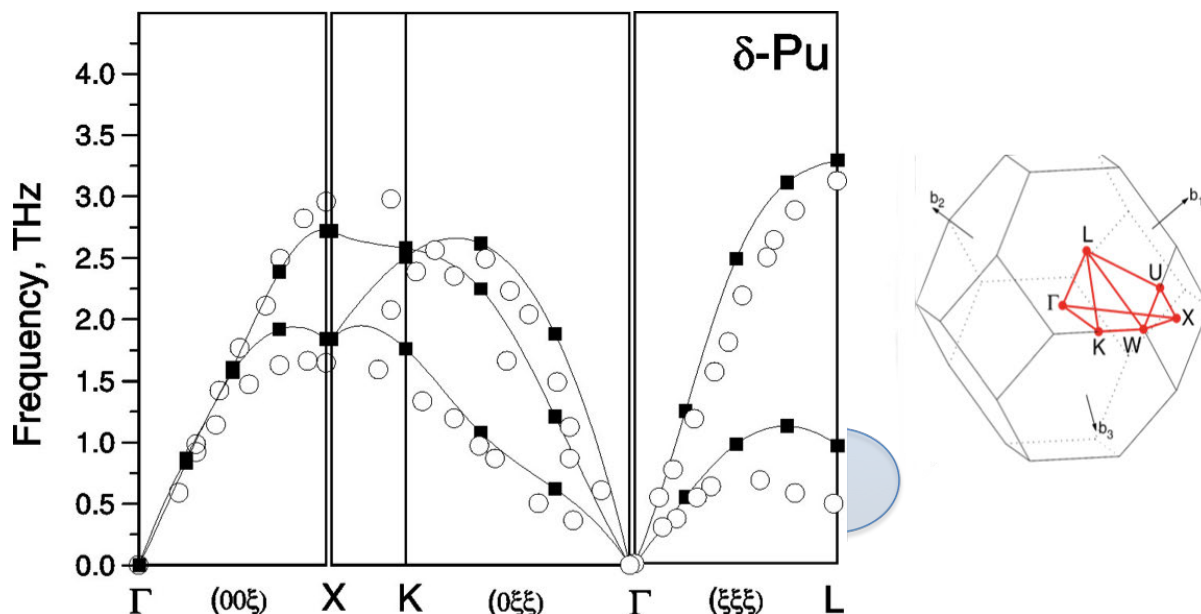


Fig. 8: Theoretical prediction for the phonon spectra of the δ -phase of Pu (empty circles) [60] and observation by inelastic X-ray scattering (black squares) [61]. The overall agreement is reasonable with maximum deviations near the L-point of the Brillouin-zone as indicated.

9 Applications: Actinides

Computation of total energies was almost exclusively the domain of density-functional theory. This can be rationalized by saying that density-functionals target the density and total energy of the material and therefore are more accurate for these quantities than for their corresponding excitation spectra. This is supported by the fact that even in materials as correlated as the high-temperature superconductors, LDA or GGA predict the structural properties with a few percent accuracy. A notable exception to this rule is provided by a $5f$ system, elemental plutonium. Nonmagnetic LDA or GGA underestimates the volume of the δ -phase by more than 30%, while allowing for magnetism gives a volume close to experiment but with a very large moment, of the order of $5\mu_B$, which is not observed experimentally. A similar problem arises in other electronic structure methods, ranging from GW to hybrid density-functionals.

The computation of total energies and phonon frequencies became possible with the introduction of the LDA+DMFT functional. The first application of charge self-consistent LDA+DMFT [59] pointed a path to solving the Pu conundrum by demonstrating that the correct volume of δ -Pu emerges from the paramagnetic LDA+DMFT calculation. Predictions for the phonon spectra [60] were largely confirmed by inelastic X-ray experiments at the ESRF.

The difference between theory and experiment highlighted in Fig. 8 focuses the research by raising interesting questions. In that early work, simplified impurity solvers were used. Hence, the calculations can be improved further. Also, temperature-dependent experimental studies should be performed, since the calculations were zero temperature calculations. Finally, effects of alloying and inhomogeneities could be investigated. This is clearly an area where theory

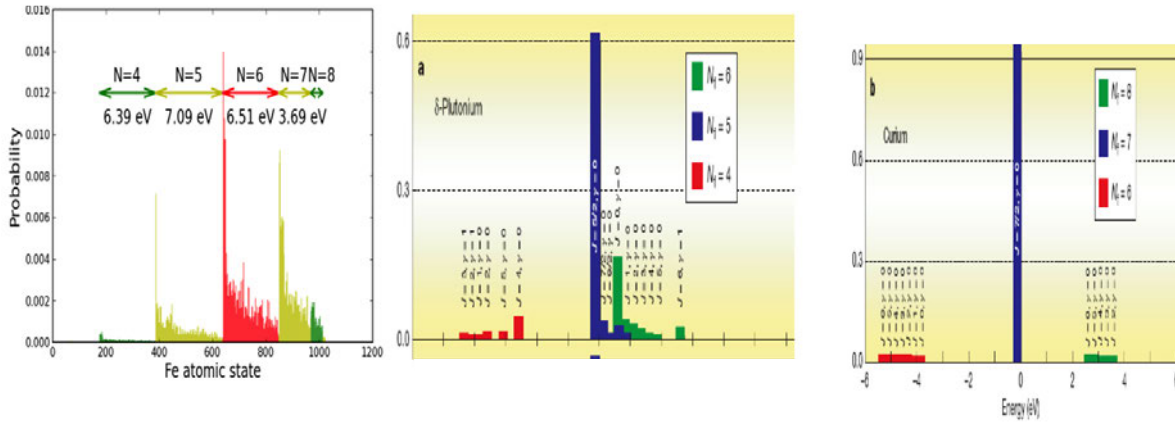


Fig. 9: LDA+DMFT valence histogram for different materials. In Cm (right) the ordinary notion of valence applies. Pu (middle) exhibits a clear mixed valence character [62]. The left panel displays the valence histogram of a Hund's metal $BaFe_2As_2$ [46].

of strongly correlated materials can continue to make important contributions to an area where experiments are very difficult.

Another important aspect of LDA+DMFT calculations is the qualitative insights they provide into the behavior of a material. Plutonium was shown to be a strongly mixed-valence system, and the absence of magnetism was explicitly demonstrated [62]. The LDA+DMFT valence histograms describe the fraction of the time that the atom spends in each atomic eigenstate. When the f -electron is very localized, there is only one atomic eigenstate that is important. This is illustrated in Fig. 9 for curium. Plutonium is very different, having appreciable fluctuations into the $5f^6$ configuration as shown in Fig. 9. The mixed valence of Pu is responsible for its unique physical properties.

The studies of Pu over the last decade illustrate very nicely the advances in the quality of the LDA+DMFT implementations. Very recently, calculations for the ground state of Pu, α -Pu, a complicated monoclinic structure with many atoms in the unit cell, were carried out, using CTQMC as an impurity solver [63].

Another recent development is the determination of the energy *vs.* volume for all the phases of Pu, carried out in Ref. [64]. It was shown that all their phases are mixed-valent. Furthermore, correcting the LDA energy with the mean-field slave-boson (or Gutzwiller) correction brings all the phases very close together in energy as highlighted in Fig. 10 (Ref. [64]). These calculations are outside the scope of what can be currently done using exact impurity solvers but are easily accessible to the formalism introduced in Sec. 2 or the equivalent (at zero temperature) Gutzwiller approximation introduced by Xi Dai and collaborators. This brings us back to the beginning of the lectures.

10 Summary and outlook

After completing the development of quantum mechanics Dirac stated that “the underlying laws necessary for the mathematical theory of the whole chemistry are thus completely known

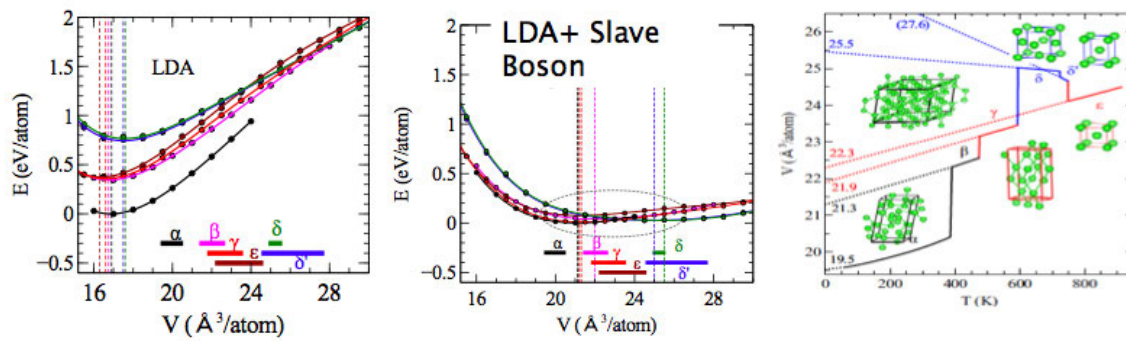


Fig. 10: *Left: Energy vs. volume of all the phases of Pu from the work of Lanatà et al. [64]. Notice that within the slave-boson method the energy differences are two orders of magnitude smaller, explaining the extreme sensitivity of the material to changes in concentration of impurities, temperature, etc. This sensitivity is highlighted in the right panel showing the experimental volume-temperature phase-diagram of Pu. The dotted lines indicate the zero-temperature equilibrium volumes extrapolated by linear interpolation. Correlations shift the region of volumes (highlighted) that becomes relevant at zero pressure. LDA already contains the relevant information about structural differences.*

and the difficulty is only that the exact application of these laws leads to equations much too complicated to be soluble.” But he proceeded to add that “approximate practical methods of applying quantum mechanics should be developed which can lead to an explanation of the main features of complex atomic systems without too much computation.”

In his famous article *More is Different* [65], P.W. Anderson, remarked that “the constructionist hypothesis breaks down when confronted with the twin difficulties of scale and complexity.” He goes on to say that “at each level of complexity entirely new properties appear, and the understanding of the new behaviors requires research which I think is as fundamental in its nature as any other,” stressing that at each level of description new concepts are needed to describe nature and there are new laws to be discovered.

Dirac and Anderson’s dictums are sometimes viewed as contradictory, but in condensed matter physics and in particular in the field of strongly correlated electrons both are needed to make progress. The quest for ideas to describe the emergent phenomena as well as the invention of techniques to compute physical properties using the basic laws of quantum mechanics of matter both play a very important role.

The developments of methodologies to treat correlated materials are an illustration of Dirac’s vision and they have lead to concepts, abstractions, and physical pictures that enable us to understand the behavior of correlated materials that are useful and will guide further studies.

There is a close interaction between scientific advances and the development of new methodologies. New methodologies enable breakthroughs in challenging scientific problems, and in turn outstanding scientific problems spur the development of new methodologies.

The development of DMFT for model Hamiltonians led to a detailed understanding of the mechanism of the Mott transition. In turn, the need to understand the Mott transition, a transition that lacks an obvious order parameter, was an important driving force for the development of DMFT.

DMFT and its extensions to clusters enabled accurate solutions of model Hamiltonians. It also gave us useful concepts for thinking about strongly correlated materials. The DMFT Weiss field makes quantitative the notion of the degree of localization of the electron. The local Green's function, with its characteristic three peak structure, gives a precise formulation of the Mott transition in terms of the transfer of one-electron spectral weight. The existence of a finite-temperature Mott transition marks a sharp boundary beyond which perturbation theory in the interactions fails.

Condensed matter theory has a dual role. On one side, it provides tools for predicting the properties of materials. On the other side, it builds the conceptual framework in which to frame and understand the results of experiments. We used two classes of materials, the actinides and the iron pnictides to illustrate the rapid progress in the field. The Pu problem was intractable with the tools of band theory, but using a combination of slave-boson and DMFT methods the determination of its phase diagram appears within sight. The iron pnictides provided a real-time demonstration of the power of the LDA+DMFT methodology for their quantitative description and at the same time resulted in a surprising discovery of a new class of strongly correlated systems. There are many more that have been studied already, and even more to be discovered. The introduction of LDA+DMFT enabled the computation of the photoemission and inverse photoemission spectra of correlated materials starting from first principles. The intensity and position of the qualitative features, already present in the model Hamiltonian, are now made quantitative and system-specific in a way that allowed comparison with experiments. The calculated spectral properties (ARPES, optics, neutron scattering, etc.) of a large number of p , $3d$, $4d$, $4f$, $5d$, and $5f$ -based materials were in surprisingly good agreement with experiments. Through the study of a very large number of materials, the community has gained confidence that we have a zeroth-order picture of strongly correlated materials, with the Kohn-Sham Hamiltonian with a double-counting correction subtracted, as a one-particle Hamiltonian and a Coulomb interaction matrix parametrized by a few Slater-Racah parameters. We have a working practical approach that gives a zeroth order-picture of correlated solids, an important challenge is to quantify its accuracy and limitations. We can start looking for deviations from this framework as well as continue to improve its implementation and foundation to increase its accuracy.

Finally it is worth reminding students that all the remarkable discoveries in strongly correlated electron materials have been the result of serendipity, and there is no reason to doubt that this will continue in the foreseeable future. Still, at this point in time, theorists working on strongly correlated electrons have in their hand sufficiently powerful tools to participate more closely in the process of understanding of these fascinating materials and accelerate their discovery. These are very exciting times to enter the field of correlated electron material research.

Acknowledgments

Research in Sec. 9 and 8 was supported by the DOE and the NSF respectively. Wenhui Xu was instrumental in the development of these notes. I thank him and K. Haule, Z. Yin, A. Kutepov, N. Lanatà, Y. Yao for collaborations and multiple discussions.

References

- [1] M.C. Gutzwiller, Phys. Rev. Lett **10**, 159 (1963)
- [2] C.M. Varma and Y. Yafet, Phys. Rev. **13**, 2950 (1976)
- [3] J. Hubbard, Proc. R. Soc. London, Ser. A **276**, 238 (1963)
- [4] K. Wilson Rev. Mod. Phys. **47**, 773 (1975)
- [5] M. Imada, A. Fujimori and Y. Tokura Rev. Mod. Phys. **70**, 1039 (1998)
- [6] A. Georges, G. Kotliar, W. Krauth, and M.J. Rozenberg, Rev. Mod. Phys. **68**, 13 (1995)
- [7] G. Kotliar *et al.*, Rev. Mod. Phys. **78**, 865 (2006)
- [8] R. Shankar, Rev. Mod. Phys. **66**, 129 (1994)
- [9] W. Kohn and L.J. Sham, Phys. Rev. **140**, A1133 (1965)
- [10] L. Hedin, Phys. Rev. **139**, A796 (1965)
- [11] S.V. Faleev, M. van Schilfgaarde, and T. Kotani, Phys. Rev. Lett. **93**, 126406 (2004)
- [12] E. Lieb and F.Y. Wu, Phys. Rev. Lett. **20**, 1445 (1968)
- [13] W. Metzner and D. Vollhardt, Phys. Rev. Lett. **62**, 324 (1989)
- [14] P.W. Anderson, Phys. Rev. **124**, 41 (1961)
- [15] G. Kotliar and A.E. Ruckenstein, Phys. Rev. Lett. **57**, 1362 (1986)
- [16] R. Fresard and G. Kotliar, Phys. Rev. B **56**, 12909 (1997)
- [17] F. Lechermann, A. Georges, G. Kotliar, and O. Parcollet, Phys. Rev. B **76**, 155102 (2007)
- [18] T. Li, P. Wölfle, and P.J. Hirschfeld, Phys. Rev. B **40**, 6817 (1989)
- [19] R. Fresard and P. Wölfle, Int. J. Mod. Phys. B **6**, 685 (1992)
- [20] R. Raimondi and C. Castellani, Phys. Rev. B. **48**, 11453(R) (1993)
- [21] N. Lanata, Y. Yao, C Wang K.M. Ho and G. Kotliar arXiv:1405.6934
- [22] A. Georges, and G. Kotliar, Phys. Rev. B **45**, 6479 (1992)
- [23] G Kotliar and D Vollhardt, Physics Today, March 2004, p. 53
- [24] E. Gull, A.J. Millis, A.I. Lichtenstein, A.N. Rubtsov, M. Troyer, and P. Werner, Rev. Mod. Phys. **83**, 349 (2011)

-
- [25] J.M. Tomczak, M. van Schilfgaarde, and G. Kotliar, Phys. Rev. Lett. **109**, 237010 (2012)
- [26] N.E. Zein, S.Y. Savrasov, and G. Kotliar, Phys. Rev. Lett. **96**, 226403 (2006)
- [27] Z.P. Yin, A. Kutepov, and G. Kotliar, Phys. Rev. X **3**, 021011 (2013)
- [28] D. Jacob, K. Haule, G. Kotliar, EPL **84**, 57009 (2008)
- [29] V.I. Anisimov, A.I. Poteryaev, M.A. Korotin, A.O. Anokhin, and G. Kotliar, J. Phys: Condens. Mat. **9**, 7359 (1997)
- [30] A.I. Lichtenstein and M.I. Katsnelson, Phys. Rev. B **57**, 6884 (1998)
- [31] S.Y. Savrasov and G. Kotliar, Phys. Rev. B **69**, 245101 (2004)
- [32] R. Chitra and G. Kotliar, Phys. Rev. B **62**, 12715 (2000)
- [33] R. Chitra, and G. Kotliar, Phys. Rev. B **63**, 115110 (2001)
- [34] I. Paul and G. Kotliar I. Paul and G. Kotliar, Eur. Phys. Jour. B **51**, 189 (2006)
- [35] J. Lee and K. Haule arXiv:1403.2474
- [36] S. Biermann F. Aryasetiawan, A. Georges PRL **90**, 086402 (2003)
- [37] P. Sun, G. Kotliar, Phys. Rev. B **66**, 085120 (2002)
- [38] P. Sun, and G. Kotliar, Phys. Rev. Lett. **92**, 196402 (2004)
- [39] K. Haule, C. H. Yee, and K. Kim, Phys. Rev. B **81**, 195107 (2010).
- [40] O.K. Andersen, Phys. Rev. B **12**, 3060 (1975)
- [41] D. J. Singh and L. Nordström: *Planewaves, Pseudopotentials and the LAPW Method* (Springer, New York, 2006)
- [42] D. van der Marel and G.A. Sawatzky, Phys. Rev. B **37**, 10674 (1988)
- [43] O. Laporte and J.R. Platt, Phys. Rev. **61**, 305 (1942)
- [44] F. Aryasetiawan, M. Imada, A. Georges, G. Kotliar, S. Biermann, and A. I. Lichtenstein, Phys. Rev. B **70**, 195104
- [45] T Miyake, F. Aryasetiawan, and M. Imada, Phys. Rev. B **80**, 155134 (2009),
- [46] A. Kutepov, K. Haule, S.Y. Savrasov, and G. Kotliar, Phy. Rev. B **82**, 045105 (2010)
- [47] A. Kutepov S. Savrasov and G. Kotliar Phys. Rev. B **80**, 041103(R) (2009)
- [48] Y. Kamihara, T. Watanabe, M. Hirano, and H. Hosono, J. Am. Chem. Soc. **130**, 3296 (2008)

- [49] K. Haule, J. H. Shim, and G. Kotliar, Phys. Rev. Lett. **100**, 226402 (2008)
- [50]] K. Haule, and G. Kotliar, New Journal of Physics **11**, 025021 (2009)
- [51] F. Hardy, A.E. Böhmer, D. Aoki, P. Burger, T. Wolf, P. Schweiss, R. Heid, P. Adelman, Y.X. Yao, G. Kotliar, J. Schmalian, and C. Meingast, Phys. Rev. Lett. **111**, 027002 (2013)
- [52] S. Florens, A. Georges, G. Kotliar, and O. Parcollet, Phys. Rev. B **66**, 205102 (2002)
- [53] M. Daybell, in *Magnetism*, pp. 122-147, Vol. 5, ed. by G. Rado and H. Suhl (Academic Press, New York, 1973)
- [54] J. R. Schrieffer, J. App. Phys. **38**, 1143 (1967)
- [55] I. Okada and K. Yosida, Prog. Theor. Phys. **49**, 1483(1973)
- [56] C. Aron and G. Kotliar, arxiv:1401.0331
- [57] Z.P. Yin, K. Haule, and G. Kotliar, Nature Mat. **10**, 932 (2011)
- [58] Z.P. Yin and G. Kotliar, Phys. Rev. B **86**, 195141 (2012)
- [59] S.Y. Savrasov, G. Kotliar, and E. Abrahams, Nature **410**, 793 (2001)
- [60] X. Dai, S.Y. Savrasov, G. Kotliar, A. Migliori, H. Ledbetter, and E. Abrahams, Science **300**, 953 (2003)
- [61] J. Wong, M. Krisch, D.L. Farber, F. Occelli, A.J. Schwartz, T.-C. Chiang, M. Wall, C. Boro, and R. Xu, Science **301**, 1078 (2003)
- [62] J.H. Shim, K. Haule, and G. Kotliar, Nature **446**, 513 (2007)
- [63] J.-X. Zhu, R.C. Albers, K. Haule, G. Kotliar, J.M. Wills Nat. Commun. **4**, 2644 (2013)
- [64] N. Lanatà, Y.X. Yao, C.Z. Wang, K.M. Ho, and G. Kotliar, arXiv:1407.4862
- [65] P.W. Anderson, Science **177**, 393 (1972)